Supplementary Information for

Real-time monitoring conformational transitions of single-molecule histone deacetylase 8 with nanocircuits

Seungyong You, James Froberg, Junru Yu, Manas Haldar, Abbas Sedigh, Sanku Mallik, D. K. Srivastava, Yongki Choi*

Department of Physics, Chemistry and Biochemistry, Pharmaceutical Science, Materials and Nanotechnology Program, North Dakota State University, Fargo, ND 58108, United States

Table of Contents

1. Materials and methods

SAHA (suberoylanilide hydroxamic acid) was custom synthesized by Biomol Laboratories (Plymouth Meeting, PA). N(phenylcarbothiol)benzamide, Coumarin-SAHA (cSAHA), Pyrene-SAHA (pSAHA), Pyrene-IDA-Cu^{2+}, and Trifluoroacetyl-lysine-coumarin conjugate (TFAL-AMC), were synthesized using previously published protocols[1-6]. All other chemicals were purchased commercially from Ezno life sciences, Biomol laboratories, Acros Organics, EMD, Fisher Scientific, or Sigma Aldrich. All regents were used as received without further purification.

The plasmid containing the coding sequence of human HDAC8 (pCMV-SPORT6) was obtained from Open Biosystem (Huntsville, Al, USA). The ligation independent cloning (LIC)-compatible Escherichia coli expression vector pLIC-HiS[7] was a kind gift from Stephen P. Bottomley (Monash University, Australia). A recombinant form of human HDAC8 was expressed and purified from Escherichia coli as described previously[2].

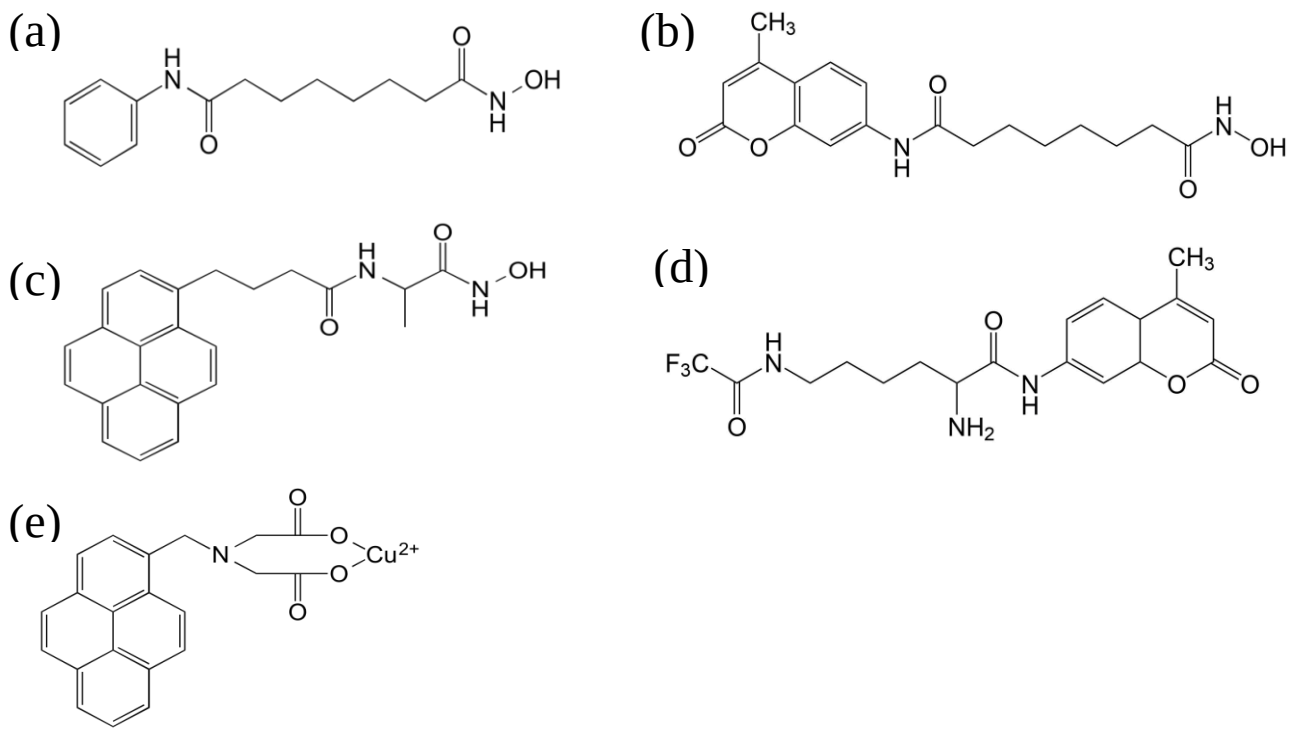

Fig. S1. Chemical structures of (a) the SAHA, (b) cSAHA, (c) pSAHA inhibitors, (d) TFAL-AMC substrate, and (e) a pyrene-IDA-Cu^{2+} linker.

2. Signal transduction mechanisms

Previously, we have proved that the SWNT-FET is extremely sensitive to electrostatic gating by the protein's charged residues within 1 nm of the attachment site[8]. When protein's loop undergoes its opening and closing motions, the movement of these charges produces a time-varying electric fields that acts in addition to the constant, externally applied gating voltage V_G to produce a time-varying change in gating ΔV_G. Considering a set of protein charges q_i dynamically varying between positions $r_{i,1}$ and $r_{i,2}$, the consequence of these charges on the SWNT current will be,

$$\Delta I = \frac{\partial I}{\partial V_G}\Delta V_G \propto \frac{\partial I}{\partial V_G}\sum_i q_i\left(\frac{1}{r_{i,1}} - \frac{1}{r_{i,2}}\right)\exp(-r_{i,1}/\lambda_D)$$

where λ_D is the Debye screening length of the electrolyte. In this equation, the variability of $\Delta I(t)$ from one device to another is entirely due to the slope $\partial I/\partial V_G$, which is an empirical, device-dependent parameter. Otherwise, the q_i and r_i terms in the above equation are entirely determined by enzyme's structure and movements[8].

Figure S2 illustrates the schematic diagram of the HDAC8-SWNT interface, showing the close-up X-ray structures of HDAC8 in its open and closed loop conformations (PDB: 3F07 and 1T64)[9]. There is uncertainty in the orientation of the HDAC8 at the SWNT, since the orientation

of the pyrene linkers and HDAC8 are not easily defined. Nevertheless, we have selected a spatially likely orientation of the HDAC8 with respect to the pyrene-SAHA in its rotational orientation that allows binding to HDAC8 to form the complex (Fig S2. (a)). The two structures were aligned using the protein backbone around the active site pocket with respect to the SAHA. In this alignment, the low current state corresponds to the motions of negatively charged tri Asp residues (87-89) in the L2 loop moving away from the SWNT during loop closing motions. Similarly, we have selected an energetically likely orientation of the pyrene-IDA linkage in its rotational orientation that allows binding to the N-terminal in one of three possible rotomers[10] (Fig. S2. (b)). With this model, the low current state could result from positively charged Arg37 and His42 residues around the N-terminal that move closer to the SWNT during the loop interactions. In both models, the fields can be calculated under the pyrene rings, where perturbation of the SWNT should lead to the most sensitive interactions, and compared to the gating ΔV_G observed experimentally to further support the orientation of HDAC8 with respect to the SWNT[8]. More detailed analysis requires precise knowledge of the pyrene linker's orientation and the SWNT's response to the fields, both of which are formidable characterization challenges.

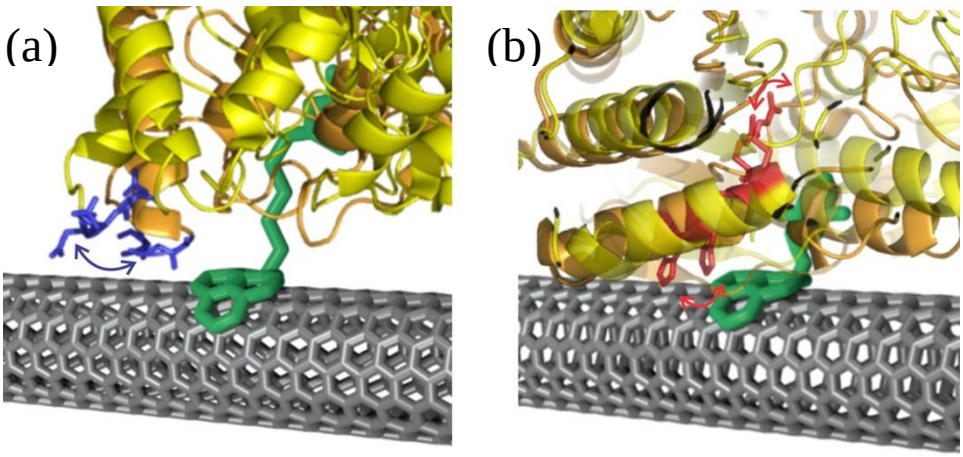

Fig. S2. Detailed view of the HDAC8-SWNT interface, showing X-ray structures of the enzyme in its open and closed conformation with (a) pSAHA-nanocircuits and (b) HDAC8-nanocircuits.

3. Dissociation off-rate measurement

The dissociation off rate of cSAHA and pSAHA from HDAC8 was determined via the stopped-flow system (Applied Photophysics). The solutions of HDAC8 (1 μM) and c-SAHA (10 μM) or pSAHA (10 μM) were mixed with 200 μM SAHA via the stopped-flow syringes. The time-dependent increase in the fluorescence signal of cSAHA due to its displacement from the enzyme site by non-fluorescent enzyme inhibitor (SAHA) was monitored using a 395-nm "cutoff" filter (λ_{ex} = 325 nm). In each experimental setup, at least 10 kinetic traces were collected and averaged. The averaged kinetic traces were analyzed by a single exponential rate equation to obtain the dissociation off-rate of cSAHA and pSAHA from HDAC8. The dissociation off rate was determined to be 21 s^{-1}.

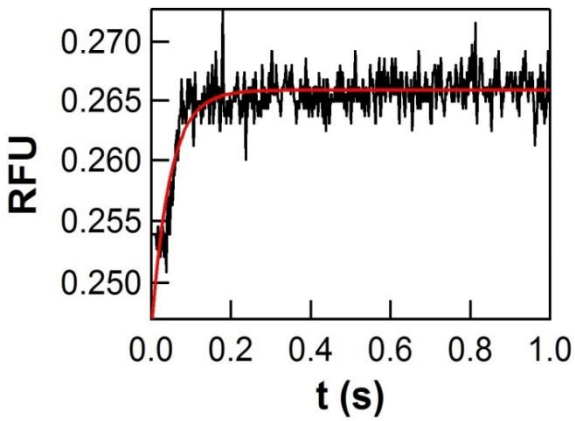

Fig. S3. Representative stopped-flow trace for the dissociation of pSAHA from the HDAC8. The red curve is the best fit of the experimental data according to the single exponential rate equation. RFU, relative fluorescence units.

4. Device fabrication and measurements

SWNTs were grown by chemical vapor deposition (CVD), followed by optical lithography for patterning electrodes and electron beam lithography for the electrodes passivation described previously[11, 12]. Devices were functionalized using a bifunctional linker molecule, either pyrene-IDA-$Cu2^{+}$ or pSAHA. The pyrene functionality adheres to the SWNT sidewall strongly via π-π stacking[13]. A solution of the linker molecules in ethanol (1 mM) was prepared. Devices were soaked in solution for 10 min without agitation, and then washed with 0.1% Tween-20 (Acros Organics) in ethanol to remove excess linker molecules. Then, the devices were rinsed under flowing either de-ionized water or a buffer (25 mM HEPES, 100 mM NaCl, 1mM TCEP, pH 7.5).

For the pSAHA measurement, a solution of HDAC8 (6 μM) was used. N(phenylcarbothiol)benzamide (6 μM) activator was mixed with HDAC8 at the ratio of 1:1, and SAHA (30 μM) was mixed with HDAC8 at the ratio of 5:1. For the cSAHA and TFAL-AMC measurements, the devices were soaked in the HDAC8 solution (1 μM) for 20 min without agitation. Next, the devices were washed thoroughly to remove unattached HDAC8. Following conjugation, devices were stored in the buffer solution and neither dried nor imaged until the completion of measurements. cSAHA (5 μM) solution was prepared and used. N(phenylcarbothiol)benzamide (20 μM) activator was mixed with cSAHA at the ratio of 1:4. TFAL-AMC (1 μM) was prepared used for TFAL-AMC measurement. Next, N(phenylcarbothiol)benzamide (20 μM) activator was mixed with TFLA at the ratio of 1:20.

All electronic measurements were performed with the active portion of the device submerged in the buffer solution. The potential of the electrolyte was controlled using Pt counter and pseudo-reference electrodes, and held at 0 ~ -0.4 V vs. Pt using Keithley 2400 sourcemeter. The source-drain bias was held at 0.1 V. A Keithley 428 preamplifier operating at 10^{8} V/A gain and with a 40 μs rise time was used to measure the source-drain current of the device. Data was collected for at least 600 s for each measurement condition. The analysis has been performed using a 10-Hz, digital low pass filter to $\Delta I(t)$ from $I(t)$[12].

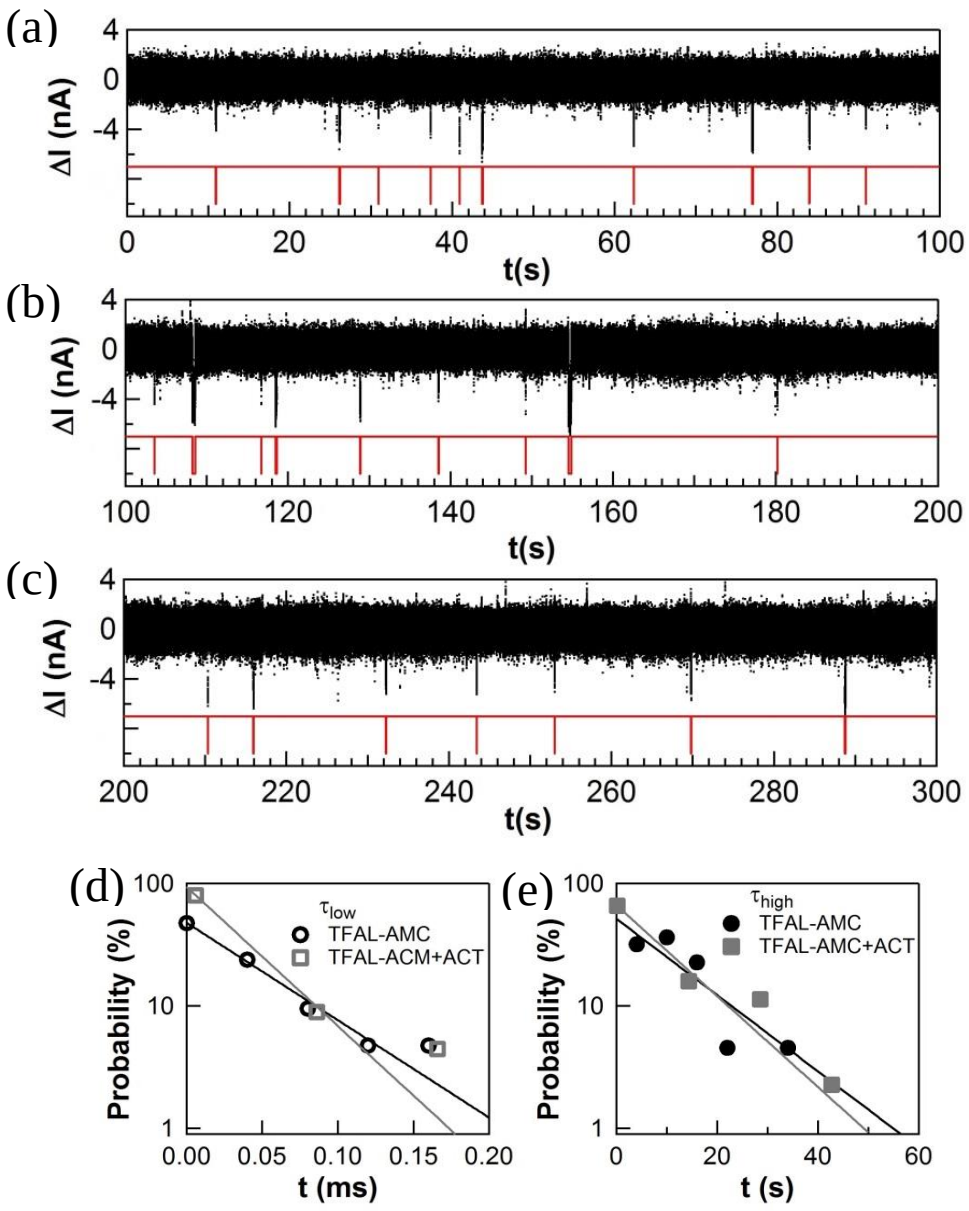

Fig. S4. Electronic monitoring of HDAC8's catalytic activities with the TFAL-AMC substrates (a)-(c). Probability distributions of the duration for two current states, (d) τ_{low} and (e) τ_{high}, accumulated from 1200 s of recordings, in the presence and absence of activators. Single exponential fits are shown as solid lines, determining the mean value of τ.

5. Steady-state kinetics of the HDAC8-catalyzed reaction

The steady-state kinetic studies for the HDAC8-catalyzed reaction were determined using a synthetic fluorogenic substrate (TFAL-AMC) via a trypsin-coupled assay as described previously[14]. The initial rate of the HDAC8-catalyzed reaction was determined in the presence of 0.25 μM HDAC8 and 3 μM trypsin as a function of the substrate concentration. The experimental data were analyzed using the Michaelis-Menten equation to determine the steady-

state kinetic parameters. The concentration of the reaction product, generated during the HDAC8-catalyzed reaction, was calculated from a standard plot of fluorescence unit versus the fluorescence product concentration under the same experimental conditions/setting used in the steady-state kinetic experiments.

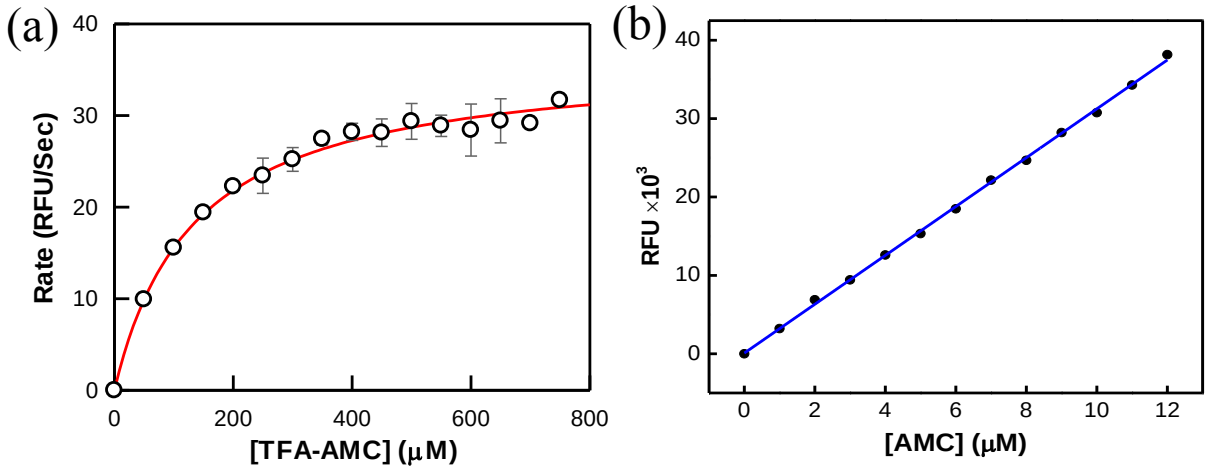

Fig. S5. (a) The initial rate of the HDAC8 catalyzed reaction as a function of substrate (TFAL-AMC) concentration. The solid line is the best fit of the data using the Michealis-Menten equation with K_m and V_{max} values of 134 ± 3 μM and 36 ± 1 RFU/sec. The V_{max} value thus derived was converted to k_{cat} (0.049 s^{-1}) using the standard curve of the fluorescence emission intensity vs. fluorophore (AMC) concentration. No effect of the activator in the same measurements was observed.

6. The mean normalized variance

The mean normalized variance $r = \sigma^2 / \langle\tau\rangle^2$ of the τ_{low}, τ_{high}, *and* τ_{high}^{long} is used to assess the number of hidden intermediate steps during the transition between closed and open loop conformations for each conditions.

	r_{low}	r_{high}	r_{high}^{long}
HDAC8	1.21 ± 0.09	1.17 ± 0.08	
HDAC8 + ACT	1.07 ± 0.07	1.30 ± 0.09	
cSAHA	0.86 ± 0.16	1.07 ± 0.19	0.48 ± 0.07
cSAHA + ACT	0.84 ± 0.13	0.93 ± 0.18	0.44 ± 0.06
TFAL-AMC	1.15 ± 0.60	0.64 ± 0.35	
TFAL-AMC + ACT	1.02 ± 0.39	0.70 ± 0.34	

Table S1. The mean normalized variance

7. References

1. R. K. Singh, T. Mandal, N. Balsubramanian, T. Viaene, T. Leedahl, N. Sule, G. Cook and D. K. Srivastava, *Bioorg Med Chem Lett*, 2011, **21**, 5920-5923.
2. R. K. Singh, T. Mandal, N. Balasubramanian, G. Cook and D. K. Srivastava, *Anal Biochem*, 2011, **408**, 309-315.
3. R. K. Singh, T. Suzuki, T. Mandal, N. Balsubramanian, M. Haldar, D. J. Mueller, J. A. Strode, G. Cook, S. Mallik and D. K. Srivastava, *Biochemistry*, 2014, **53**, 7445-7458.
4. D. Riester, D. Wegener, C. Hildmann and A. Schwienhorst, *Biochem Biophys Res Commun*, 2004, **324**, 1116-1123.
5. H. El Bakkali, D. Choquesillo-Lazarte, A. Domínguez-Martín, M. I. Pérez-Toro, L. Lezama, J. M. González-Pérez, A. Castiñeiras and J. Niclós-Gutiérrez, *Crystal Growth & Design*, 2014, **14**, 889-892.
6. A. L. Banerjee, M. Swanson, B. C. Roy, X. Jia, M. K. Haldar, S. Mallik and D. K. Srivastava, *J. Am. Chem. Soc.*, 2004, **126**, 10875-10883.
7. L. D. Cabrita, W. Dai and S. P. Bottomley, *BMC Biotechnology*, 2006, **6**, 12-12.
8. Y. Choi, T. J. Olsen, P. C. Sims, I. S. Moody, B. L. Corso, M. N. Dang, G. A. Weiss and P. G. Collins, *Nano Lett.*, 2013, **13**, 625-631.
9. N. Deschamps, C. A. Simoes-Pires, P. A. Carrupt and A. Nurisso, *Drug Discov Today*, 2015, **20**, 736-742.
10. H. Schrauber, F. Eisenhaber and P. Argos, *J. Mol. Biol.*, 1993, **230**, 592-612.
11. B. R. Goldsmith, J. G. Coroneus, V. R. Khalap, A. A. Kane, G. A. Weiss and P. G. Collins, *Science*, 2007, **315**, 77-81.
12. Y. Choi, I. S. Moody, P. C. Sims, S. R. Hunt, B. L. Corso, G. A. Weiss and P. G. Collins, *Science*, 2012, **335**, 319-324
13. R. J. Chen, Y. Zhang, D. Wang and H. Dai, *J. Am. Chem. Soc.*, 2001, **123**, 3838-3839.
14. R. K. Singh, K. Cho, S. K. Padi, J. Yu, M. Haldar, T. Mandal, C. Yan, G. Cook, B. Guo, S. Mallik and D. K. Srivastava, *J. Biol. Chem.*, 2015, **290**, 6607-6619.